



# Effect of pyrolysis temperature on characteristics of biochars derived from different feedstocks: A case study on ammonium adsorption capacity



Defu Xu <sup>a,b,c,d,\*</sup>, Junmin Cao <sup>a,c</sup>, Yingxue Li <sup>a</sup>, Alan Howard <sup>e</sup>, Kewei Yu <sup>f</sup>

<sup>a</sup> Collaborative Innovation Center of Atmospheric Environment and Equipment Technology, Nanjing 210044, China

<sup>b</sup> Key Laboratory of Agro-Environment in downstream of Yangze Plain, Ministry of Agriculture, China

<sup>c</sup> Jiangsu Key Laboratory of Atmospheric Environment Monitoring and Pollution Control, Nanjing 210044, China

<sup>d</sup> School of Environmental Science and Engineering, Nanjing University of Information Science & Technology, Nanjing 210044, China

<sup>e</sup> Department of Geography and Environmental Science, University of Reading, Reading RG6 6AB, UK

<sup>f</sup> Department of Biological and Environmental Sciences, Troy University, Troy, AL 36082, USA

## ARTICLE INFO

### Article history:

Received 24 August 2018

Revised 6 January 2019

Accepted 28 February 2019

### Keywords:

Biochar  
Pyrolysis temperature  
Ammonium  
Adsorption

## ABSTRACT

Physicochemical properties of biochars derived from different feedstock materials (rice straw, *Phragmites communis*, sawdust and egg shell) at different pyrolysis temperatures were analyzed, and adsorption capacities of ammonium ( $\text{NH}_4^+$ ) on the biochars were investigated. The results show a clear effect of pyrolysis temperature on physicochemical properties of the biochars, including specific surface area, pH, and zeta potential. Consequently, biochars derived from the studied feedstocks at the selected temperatures exhibited different capacities to absorb  $\text{NH}_4^+$ . Highest  $\text{NH}_4^+$  adsorption capacities were associated with biochars of rice straw (4.2 mg/g) and sawdust (3.3 mg/g) produced at 500 °C; at 300 °C observed  $\text{NH}_4^+$  adsorption capacity was lower and highest figures were derived from the biochars of *Phragmites communis* (3.2 mg/g) and egg shell (2.2 mg/g). For all feedstocks, biochars produced at 700 °C showed the lowest  $\text{NH}_4^+$  adsorption capacity. Our results suggest that zeta potential and C/H ratio, rather than surface area, are the most important factors in determining  $\text{NH}_4^+$  sorption potential of biochars.

© 2019 Elsevier Ltd. All rights reserved.

## 1. Introduction

Human activities such as discharging agricultural and industrial wastewaters lead to rapid increases in nitrogen (N) loadings in aquatic ecosystems (Yin et al., 2018). Leaching and run-off of ammonium ( $\text{NH}_4^+$ ) from agriculture decreases utilization efficiency of N fertilizer, and therefore exacerbates the risk of eutrophication (Li et al., 2018) and degradation of aquatic ecosystems (Smith, 2003). Ammonium is the most common form of N, contributing to nutrient enrichment of surface waters (Conley et al., 2009). Hence, it is necessary to enhance N retention in agricultural soils and  $\text{NH}_4^+$  removal from water to protect water resources and maintain a healthy aquatic ecosystem (Cui et al., 2016).

Several technologies (e.g. biological, chemical and physical methods) have been used to remove  $\text{NH}_4^+$  from wastewater. Physical methods are often used due to their simpler practical operation and easier management (Loganathan et al., 2014). Sorption is also

considered an effective physical method and is relatively low cost (Sun et al., 2011). Adsorbents, such as zeolite, aluminum oxide and activated carbon, efficiently remove ammonium from wastewater (Cui et al., 2016). Although  $\text{NH}_4^+$  adsorption capacity varies between different adsorbents, use of these low-cost and high-effective materials in wastewater treatment is promising and has received increasing attention (Li et al., 2017a, 2017b).

Many kinds of biomass waste, such as agricultural wastes, forestry residues and sewage sludge, can be used to produce biochar (Li et al., 2017a, 2017b; Kizito et al., 2015; Zhang and Wang, 2016). Using these materials is relatively low cost compared to using activated carbon (Tarpeh et al., 2017), and can decrease air pollution and reduce fire risks that may arise from uncontrolled burning of biomass waste (Qiu et al., 2016).

Biochar's characteristics can affect its adsorption capacity to contaminants. The potential adsorption capacity of different biochars vary depending on the specific characteristics of the feedstock used (Yin et al., 2018). For example, addition of Brazilian pepper wood and peanut hull biochars to soil considerably reduced leaching of  $\text{NO}_3^-$  by 14.0–34.0% (Yao et al., 2012). However, in another study, Hale et al. (2013) used biochars, such as cacao shell

\* Corresponding author at: School of Environmental Science and Engineering, Nanjing University of Information Science & Technology, Nanjing 210044, China.  
E-mail address: [defuxu1@163.com](mailto:defuxu1@163.com) (D. Xu).

and corn cob biochars, that were found not to adsorb  $\text{NO}_3^-$ . More information is needed on  $\text{NH}_4^+$  sorption capacity of different feedstock materials and the effect of pyrolysis temperature. Therefore, the aims of this study were (1) to analyze characteristics of biochars produced from different feedstocks at different pyrolysis temperatures; (2) to determine the sorption capacity of  $\text{NH}_4^+$  and (3) to analyze the correlations between biochar's characteristics and sorption capacities for  $\text{NH}_4^+$ . Results of this study are expected to reveal some mechanisms of  $\text{NH}_4^+$  sorption on biochars.

## 2. Materials and methods

### 2.1. Biochar preparation

Feedstock materials used for the study - rice straw, *Phragmites communis*, and egg shell - were obtained from Nanjing University of Information Science and Technology, Nanjing, China. Sawdust was obtained from a Chinese parasol tree (*Firmiana platanifolia Marsili*), a deciduous tree species in the Yangtze river basin of China. These materials were washed with water, and then air-dried, ground and sieved to <2.0 mm particles. The sieved materials were put in a ceramic pot in a muffle furnace under  $\text{N}_2$  atmosphere for producing biochars at different temperatures. The final pyrolysis temperatures were selected to be 300, 500 and 700 °C at a ramping rate of 5 °C per min, respectively, and kept at the highest temperature for 2 h. The biochars produced under 300, 500 and 700 °C, are referred to as RSB300, RSB500, RSB700 (from rice straw), PCB300, PCB500, PCB700 (from *Phragmites communis*), SDB300, SDB500, SDB700 (from sawdust), and ESB300, ESB500, ESB700 (from egg shell), respectively (Fig. 1). Each of the 12 biochar samples were ground, and then passed through a 0.5-mm sieve to prepare for the test.

### 2.2. Characterization of biochar

Moisture content was measured by calculating mass loss of the biochar after being heated at 105 °C for 24 h to a constant weight. Ash content was also determined by calculating mass loss of the biochar after being heated at 750 °C for 5 h. The pH was determined in solution with mass/water (biochar/deionized water) ratio of 1:20 (PHS-3C). Elemental composition (C, H, and N in wt%) of the biochar was determined through an elemental analyzer whereas O content (wt%) was determined by mass balance: i.e.,  $\text{O} = 100 - (\text{C} + \text{H} + \text{N} + \text{ash})$  (Li et al., 2018). In this study, the C, H and N content was analyzed using a CHN Elemental Analyzer (Vario EL). The oxygen content was determined by mass balance:  $\text{O} = 100 - (\text{C} + \text{H} + \text{N} + \text{ash})$ . The H/C, O/C and (O+N)/C atomic ratios were calculated to evaluate the aromaticity and polarity of the biochars, respectively.

Surface functional groups of the biochar were analyzed using the fourier transform infrared analysis (Nicolet iS5). The specific surface area and porosity properties of the biochars were determined by using the Brunauer-Emmett-Teller (BET) method with a Quadrasorb Si-MP surface area analyzer. Zeta-potential at pH 7 was determined with a potential analyzer (Zetasizer Nano ZS90).

### 2.3. Adsorption kinetics experiments

Ammonium chloride was dissolved in deionized water to make an ammonium stock solution. The initial pH for each sorption solution was adjusted to 7 prior to the experiments. A 0.2 g biochar sample was added to a centrifuge tube with 20 mL solution containing 30 mg  $\text{NH}_4^+$  per L. Subsamples were taken after 30, 60, 180, 300, 420, 780, 1080 and 1440 min and shaken at 180 rpm in a mechanical shaker at room temperature (30 °C). The  $\text{NH}_4^+$  content of the subsamples was measured at a wavelength of 697 nm with a spectrophotometer according to the salicylic acid method (Ministry of Environmental Protection, 2006).

The amount of  $\text{NH}_4^+$  adsorbed by the biochars was calculated by the following equation (Eq. (1))

$$q_t = \frac{(C_0 - C_t) \times V}{W} \quad (1)$$

where  $q_t$  (mg/g) is the amount of  $\text{NH}_4^+$  adsorbed by the biochar at the given time;  $C_0$  and  $C_t$  (mg/L) are the  $\text{NH}_4^+$  concentration before and after adsorption at time  $t$ , respectively;  $V$  (L) is the volume of adsorption solution; and  $W$  (g) is the weight of biochar.

The experimental results were fitted to three typical kinetic models (Pseudo-first-order Eq. (2)), Pseudo-second-order Eq. (3) and Intraparticle diffusion Eq. (4).

$$\ln(q_e - q_t) = \ln q_e - K_1 t \quad (2)$$

$$\frac{t}{q_t} = \frac{1}{K_2 q_e^2} + \frac{t}{q_e} = \frac{1}{h} + \frac{t}{q_e} \quad (3)$$

$$q_t = K_3 t^{0.5} + C \quad (4)$$

where  $q_e$  (mg/g) is the amounts of  $\text{NH}_4^+$  adsorbed by the biochar at the equilibrium time;  $K_1$  (1/h),  $K_2$  (g/mg/h), and  $K_3$  (mg/g/h<sup>0.5</sup>) are the rate constants of the corresponding model; and  $C$  (mg/g) is a constant.

### 2.4. Adsorption isotherm experiment

Sorption isotherms of  $\text{NH}_4^+$  were measured using a series of batch experiments in centrifugal tubes containing different concentrations of  $\text{NH}_4^+$ , ranging from 0 to 320 mg/L (0, 5, 10, 20, 40, 80, 160 and 320 mg/L). Sorption isotherm condition was the same as above. After being shaken for 24 h, the suspensions were cen-

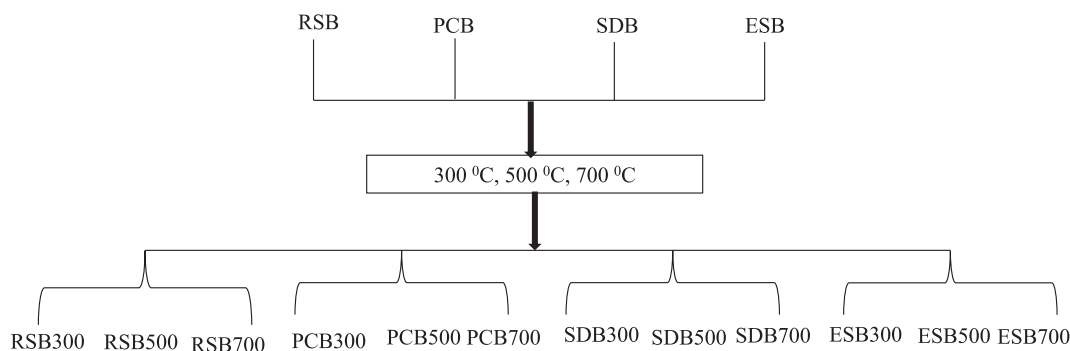


Fig. 1. Schematic setup of the biochar production.

trifuged and filtered to obtain the supernatant solution for analysis of  $\text{NH}_4^+\text{-N}$ . Concentration of  $\text{NH}_4^+\text{-N}$  was calculated according to Eq. (5).

$$q = \frac{(C_0 - C_e) \times V}{W} \quad (5)$$

where  $q$  (mg/g) is the adsorbed amount of  $\text{NH}_4^+$  per unit weight of biochar at an equilibrium concentration of adsorbate in bulk solution;  $V$  (L) is the volume of  $\text{NH}_4^+$  solution;  $W$  (g) is the weight of biochar;  $C_0$  (mg/L) and  $C_e$  (mg/L) is the initial and equilibrium  $\text{NH}_4^+$  concentration, respectively.

Sorption isotherms were fitted to the Langmuir (Eq. (6)) and Freundlich (Eq. (7)) equations to quantify the adsorption capacities of the studied biochars.

$$q = \frac{q_{\max} K_L C_e}{1 + K_L C_e} \quad (6)$$

$$q = K_F C_e^{1/n} \quad (7)$$

where  $q$  (mg/g) and  $C_e$  (mg/L) are the same as above;  $1/n$  is the intensity of adsorption or affinity;  $q_{\max}$  (mg/g) is the maximum sorption capacity;  $K_F$  (mg/g) and  $K_L$  (L/mg) are Freundlich adsorption constant and Langmuir constant, respectively.

## 2.5. Adsorption thermodynamics

Sorption data of RSB500, PCB300, SDB500, and ESB300 using initial  $\text{NH}_4^+\text{-N}$  concentration (20, 40, 80, 160 and 320 mg/L) at a temperature range of 20, 30 and 40 °C were collected after 24 h equilibration time.

The thermodynamic equilibrium constant  $K_c$  was calculated by the following equation:

$$K_c = \frac{C_0 - C_e}{C_e}$$

where  $C_0$  and  $C_e$  (mg/L) are the same as above.

Three parameters (Gibb's free energy change ( $\Delta G^\circ$ ), enthalpy change ( $\Delta H^\circ$ ) and entropy change ( $\Delta S^\circ$ )) were calculated:

$$\Delta G^\circ = -RT \ln K_c$$

$$\ln K_c = -\frac{\Delta G^\circ}{RT} = -\frac{\Delta H^\circ}{RT} + \frac{\Delta S^\circ}{R}$$

where,  $T$  is temperature in K,  $R$  the ideal gas constant = 8.314 J/mol/K.

After the linear plot of  $\ln K_c$  versus  $1/T$ , the enthalpy ( $\Delta H^\circ$ ) and entropy ( $\Delta S^\circ$ ) values could be calculated from the slope ( $\Delta H^\circ/RT$ ) and intercept ( $\Delta S^\circ/R$ ), respectively.

## 2.6. Statistical analysis

All experiments were conducted in triplicate. Correlations between the maximum adsorption of  $\text{NH}_4^+$  and physicochemical characteristic of the biochars were analyzed using SPSS 22.0. The origin Pro 8.0 was used to fit the kinetics and isotherms sorption, and  $R^2$  values were used to evaluate the performance of different models.

## 3. Results and discussion

### 3.1. Yields, ash, pH and zeta potential for different biochars with different pyrolysis temperatures

Biochar, bio-oil and syn-gas can be produced in pyrolysis of feedstocks, and there is a mass balance (i.e., feedstock = biochar

+ bio-oil + syn-gas) (Li et al., 2018). In this study, the biochar was collected as the solid residue after pyrolysis. Rice straw, sawdust, and *Phragmites communis* are forms of plant waste. Egg shell is a waste from daily life, and its annual production is about 3.7 million tonnes in China (He et al., 2016). Yields of the biochar varied with different feedstocks and pyrolysis temperatures and are presented in Table 1. Egg shell had a higher biochar yield, in a range of 93.75% to 97.4%, than those from rice straw, sawdust, and *Phragmites communis* produced at the same pyrolysis temperatures. Inorganic compounds ( $\text{CaCO}_3$ ) are major components of egg shell and result in higher yield of biochar. As shown in Table 1, biochar yields of the plant wastes (RSB, PCB and SDB) significantly decreased in pyrolysis from 300 °C to 700 °C. Anastasakis et al. (2011) reported that the cellulose of marine brown macroalgae can be thermally decomposed over 200 °C. Jung et al. (2016) demonstrated a decrease in yield for biochar from roots of *Undaria pinnatifida* when the pyrolysis temperature changed from 200 to 800 °C mainly attributed to the destruction of cellulose. Therefore, the lower biochar yield from the plant wastes under the pyrolysis temperature of 700 °C of this study could be related to destruction of the cellulose.

According to Table 1, ash contents of the biochars were influenced by feedstock materials and pyrolysis temperatures. Except for ESB, the ash contents of plant waste biochars significantly increased when the pyrolysis temperature increased from 300 °C to 700 °C. The ash content increased from 19.14% to 39.04% for RSB300 and RSB700, and similar results were found for PCB and SDB. Zhang et al. (2015a, 2015b) reported that the ash was remained in the biochars produced from biomass wastes. Therefore, the increased percentage of ash content for these biochars under higher pyrolysis temperature is attributed to more mineral matter forming ashes. However, ash content of ESB was not significantly changed by increasing the pyrolysis temperatures. Ash content of the biochars followed the order of ESB > RSB > PCB > SDB. In this study, the yields and ash contents of ESB were higher compared to other biochars, which may be attributed to a larger amount of minerals in egg shell.

Table 1 showed that higher pH values of the biochars produced under higher pyrolysis temperatures were observed. The pH of plant waste biochars (RSB, PCB and SDB) changed from acidic to alkaline at pyrolysis temperature of 300 °C to 700 °C, respectively. Our results agree with Zhang et al. (2015a, 2015b), who demonstrated that an oak wood biochar was acid (4.60) and alkaline (9.50) when it was produced at 200 °C and 600 °C, respectively. The higher pH of biochar could be attributed to its ash component (Jin et al., 2016; Yuan et al., 2011). Therefore, accumulated ash content of the biochar contributed to the increase in pH when the pyrolysis temperature increased from 300 °C to 700 °C. The pH value of ESB was neutral to alkaline at pyrolysis temperature of 300 °C to 700 °C. This is also ascribed to accumulated ash content in the biochar (Chen et al., 2014).

Zeta-potentials of the studied biochars were negative (Table 1), and the least negative charge was obtained in the biochars produced at pyrolysis temperature of 700 °C. The similar results were found by Yuan et al. (2011), who demonstrated that the negative charge was less for the biochars produced at pyrolysis temperature of 700 °C than those produced at 300 °C and 500 °C. ESB had the lower negative charge comparing to those of other biochars. The reduced amounts of negatively charged functional groups including  $-\text{COO}^-$ ,  $-\text{COH}$ , and  $-\text{OH}$ , resulted in decreasing negative surface charges of the biochars under higher pyrolysis temperatures.

### 3.2. Elemental compositions of different biochars

The C contents increased from 36.4%, 37.4% and 55.9% in RSB300, PCB300 and SDB300 to 54.1%, 59.2% and 71.7% in

**Table 1**  
Yield, ash content, pH and zeta potential of the studied biochars.

Biochar	Yield (%)	ash (%)	pH	Zeta potential (mV)
RSB300	46.31 ± 0.99a	19.14 ± 0.02a	6.61 ± 0.05a	−30.50 ± 0.70a
RSB500	25.64 ± 1.33b	32.20 ± 0.13b	9.28 ± 0.07b	−41.90 ± 1.05b
RSB700	18.66 ± 2.01c	39.04 ± 0.52c	10.06 ± 0.1c	−19.35 ± 1.92c
PCB300	43.16 ± 1.08a	4.18 ± 0.24a	6.43 ± 0.03a	−39.30 ± 0.76a
PCB500	20.89 ± 1.26b	14.97 ± 0.06b	6.82 ± 0.02b	−30.33 ± 2.01b
PCB700	14.70 ± 0.73c	15.62 ± 0.02b	9.42 ± 0.04c	−23.41 ± 0.70c
SDB300	46.80 ± 0.78a	1.2 ± 0.01a	4.55 ± 0.14a	−25.63 ± 0.54a
SDB500	19.54 ± 1.54b	2.18 ± 0.01a	6.03 ± 0.02b	−39.90 ± 1.20b
SDB700	13.85 ± 1.15c	3.12 ± 0.02b	7.88 ± 0.08c	−16.60 ± 0.29c
ESB300	97.4 ± 0.18a	98 ± 0.11a	7.89 ± 0.04a	−9.99 ± 0.92a
ESB500	95.85 ± 0.20b	98.01 ± 0.1a	8.02 ± 0.11a	−4.94 ± 1.63b
ESB700	93.75 ± 0.13c	99 ± 0.09a	9.46 ± 0.07b	−2.99 ± 1.37b

RSB300, RSB500 and RSB700 represent rice straw biochar produced at 300 °C, 500 °C and 700 °C, respectively. PCB300, PCB500 and PCB700 represent *Phragmites communis* biochar produced at 300 °C, 500 °C and 700 °C, respectively. SDB300, SDB500 and SDB700 represent sawdust biochar produced at 300 °C, 500 °C and 700 °C, respectively; ESB300, ESB500 and ESB700 represent egg shell biochar produced at 300 °C, 500 °C and 700 °C, respectively. Data are means ± SD (n = 3). Different letters in the same column indicate significant differences in temperature treatments for each biochar (p < 0.05).

**Table 2**  
Elemental compositions of the studied biochars.

Biochar	N (%)	C (%)	H (%)	O (%)	H/C	O/C	(O + N)/C
RSB300	1.36	36.40	4.06	58.18	0.11	1.60	1.64
RSB500	1.12	42.57	3.22	53.09	0.08	1.25	1.27
RSB700	0.30	54.06	1.31	44.33	0.02	0.82	0.83
PCB300	0.42	37.39	4.28	57.91	0.11	1.55	1.56
PCB500	0.14	55.19	4.17	40.50	0.08	0.73	0.74
PCB700	0.12	59.15	3.51	37.22	0.06	0.63	0.63
SDB300	0.02	55.90	4.60	39.48	0.08	0.71	0.71
SDB500	0.01	64.07	3.18	32.74	0.05	0.52	0.51
SDB700	0.00	71.72	2.97	25.31	0.04	0.35	0.35
ESB300	0.11	23.59	0.70	75.60	0.03	3.20	3.21
ESB500	0.03	15.93	0.25	83.79	0.02	5.26	5.26
ESB700	0.09	14.83	0.18	84.90	0.01	5.72	5.73

RSB300, RSB500 and RSB700 represent rice straw biochar produced at 300 °C, 500 °C and 700 °C, respectively. PCB300, PCB500 and PCB700 represent *Phragmites communis* biochar produced at 300 °C, 500 °C and 700 °C, respectively. SDB300, SDB500 and SDB700 represent sawdust biochar produced at 300 °C, 500 °C and 700 °C, respectively; ESB300, ESB500 and ESB700 represent egg shell biochar produced at 300 °C, 500 °C and 700 °C, respectively.

RSB700, PCB700 and SDB700, respectively. The result suggests a higher carbonization for biochars at higher temperature. However, the H, N, and O contents were lower for the plant wastes (RSB, PCB and SDB) produced at pyrolysis temperature of 700 °C than at 300 °C. Our results are similar to previous studies, including Jung et al. (2016) who demonstrated that C content was higher for a biochar produced at higher pyrolysis temperature. Fang et al. (2014) reported that the decreasing H, N and O content could be attributed to the loss of these elements when a biochar was made. However, the C content in ESB300 decreased from 23.6% to 14.8% in ESB700, and the O content in ESB300 increased from 75.6% to 84.9% in ESB700. Therefore, the effect of pyrolysis temperature on the C and O contents in ESB was different to that for RCB, PCB and SDB. Chun et al. (2004) found that O and H functional groups were removed from the surface of biochars produced at higher pyrolysis temperature, resulting in decrease in acidity and increase in aromaticity and hydrophobicity. In this study, results show that the acidity and polarity of RSB, PCB and SDB decreased with increasing pyrolysis temperature.

Molar H/C and O/C or (O + N)/C have been used to estimate the aromaticity and polarity of biochars (Uchimiya et al., 2010). The H/C ratios of RSB700, PCB700 and SDB700 were 0.02, 0.06 and 0.04, respectively, indicating that there is higher aromaticity for the biochars produced at 700 °C compared to at 300 °C. This is similar to those of Jung et al. (2016), who demonstrated that the H/C value was the lowest in biochars produced at pyrolysis temperature of 800 °C than at 200 °C. In this study, ESB700 showed the lowest H/C ratio of 0.01. Chen et al. (2008) indicated that

relatively higher H/C ratios were related to presence of original organic residues. Therefore, ESB with lower H/C ratios could be due to lower original organic residues, as compared to RSB, PCB and SDB.

The ratios of O/C and (O + N)/C decreased in the biochars (RSB700, PCB700 and SDB700) produced at pyrolysis temperature of 700 °C than at 300 °C, indicating an increase in aromaticity and decrease in polarity for the biochars produced at higher pyrolysis temperature. This change in aromaticity and polarity could be attributed to formation of aromatic structures and removal of polar functional groups for biochars produced at a higher pyrolysis temperature (Ahmad et al., 2012; Chen et al., 2008; Uchimiya et al., 2010). Jung et al. (2016) showed that a biochar produced at a higher pyrolysis temperature presented a lower O/C ratio, and the lowest (O + N)/C ratio was found in the biochar produced at pyrolysis temperature of 800 °C. Our results are similar to these previous studies. However, the molar O/C and (O + N)/C ratios were lower in ESB300 than in ESB700. Therefore, the H/C, O/C and (O + N)/C ratios were different in different feedstock materials, and were also influenced by pyrolysis temperatures.

### 3.3. Specific surface area and total volume of biochars

Specific surface area and total volume of the biochars were influenced by different feedstock materials and pyrolysis temperatures. They were significantly higher for the biochars produced at 700 °C than at 300 °C (Table 3). The formed micropores and increased surface area were related to the removal of volatile matters from the biochars and water loss in the dehydration process at

**Table 3**  
Porosity properties of the studied biochars.

Biochar	Total volume (cm <sup>3</sup> /g)	Specific surface area (m <sup>2</sup> /g)
RSB300	0.022	5.896
RSB500	0.072	34.030
RSB700	0.189	122.625
PCB300	0.008	3.512
PCB500	0.106	131.457
PCB700	0.415	441.710
SDB300	0.006	2.946
SDB500	0.233	378.718
SDB700	0.278	594.920
ESB300	0.004	2.032
ESB500	0.006	3.720
ESB700	0.009	5.333

RSB300, RSB500 and RSB700 represent rice straw biochar produced at 300 °C, 500 °C and 700 °C, respectively. PCB300, PCB500 and PCB700 represent *phragmites communis* biochar produced at 300 °C, 500 °C and 700 °C, respectively. SDB300, SDB500 and SDB700 represent sawdust biochar produced at 300 °C, 500 °C and 700 °C, respectively; ESB300, ESB500 and ESB700 represent egg shell biochar produced at 300 °C, 500 °C and 700 °C, respectively.

high temperature (Mahtab et al., 2012; Bagreev et al., 2001). Our results agreed with those of Chen et al. (2014), who indicated that porosity and surface area of biosolids biochar increased from 0.056 to 0.099 cm<sup>3</sup>/g and from 25.4 to 67.6 m<sup>2</sup>/g respectively, when pyrolysis temperature was increased from 500 °C to 900 °C. Therefore, the surface area and total volume of the biochars were influenced by pyrolysis temperatures.

ESB showed a smaller surface area (5.333 m<sup>2</sup>/g) and total volume (0.009 cm<sup>3</sup>/g), but SDB produced at 700 °C showed a larger surface area (594.920 m<sup>2</sup>/g) and total volume (0.278 cm<sup>3</sup>/g). Li et al. (2017a, 2017b) demonstrated that manure and biosolid biochar presented much smaller surface area (5.4–94.2 m<sup>2</sup>/g), compared to plant biochars such as wheat and wood (112–642 m<sup>2</sup>/g). In addition, Joseph et al. (2007) showed that a biosolid biochar had a smaller porosity (0.053–0.068 cm<sup>3</sup>/g) than a pine needle biochar (0.076–1.90 cm<sup>3</sup>/g) produced at temperature of 500–700 °C. Generally, a macroporous structure was developed for biochars produced from feedstocks with rich lignin content such as bamboo and coconut shell, while a microporous structure was predominantly developed for feedstocks with rich cellulose content (e.g., husks) (Li et al., 2017a, 2017b). In this study, the results show that the smaller specific surface area in ESB was due to less lignin and cellulose. Therefore, surface area of biochars can be influenced by the composition of feedstock materials.

### 3.4. Sorption kinetics

Ammonium sorption on the biochars reached equilibrium in 7 h. Ammonium sorption in the initial 1 h was fast for RSB, PCB and SDB (Fig. 2a–c), but ammonium sorption by ESB in the initial 3 h was relatively fast (Fig. 2d).

Kinetic models have been commonly used to study sorption reaction mechanisms (Wang et al., 2011). The kinetic parameters of NH<sub>4</sub><sup>+</sup> sorption on the studied biochars were shown in Table 4. Except for RSB700, the sorption data were well fitted to the pseudo-second-order kinetic model for the biochars with a higher R<sup>2</sup> in a range of 0.939–1.0. However, the adsorption data didn't fit the intra-particle diffusion well with a low R<sup>2</sup> between 0.469 and 0.822 (Table 4), indicating that intrapore diffusion was not the dominant process of NH<sub>4</sub><sup>+</sup> sorption. Wang et al. (2015) indicated that the pseudo-second-order model implied chemical reactions including exchange of cations, complexation and precipitation. In this study, the NH<sub>4</sub><sup>+</sup> sorption by biochar could be mainly of chemical adsorption process.

### 3.5. Sorption isotherms

It can be seen from Fig. 3 that among the four biochars, RSB showed the highest sorption capacity for NH<sub>4</sub><sup>+</sup>, whereas sorption NH<sub>4</sub><sup>+</sup> capacity on ESB was the lowest. The amount of sorption NH<sub>4</sub><sup>+</sup> was lower at pyrolysis temperature 700 °C than at 300 °C or 500 °C. High correlation coefficients of 0.934–0.998 (Table 5), suggest that adsorption data fits better to the Langmuir equation than to the Freundlich equation. Our results were similar to those of Tan et al. (2008), who reported that the adsorption data fitted to the Langmuir equation well.

The maximum sorption of NH<sub>4</sub><sup>+</sup> ( $q_{\max}$ ) was lower in the biochar produced at 700 °C than at 500 °C or 300 °C, indicating that the maximum sorption of NH<sub>4</sub><sup>+</sup> decreased under higher pyrolysis temperature. The maximum sorption of NH<sub>4</sub><sup>+</sup> ( $q_{\max}$ ) on RSB300, PCB300, SDB300 and ESB300 was 4.09, 3.206, 3.169 and 2.201 mg/g, respectively. The  $q_{\max}$  on RSB300 was approximately 2 times higher than that of ESB300. The results show that the sorption capacity of NH<sub>4</sub><sup>+</sup> was influenced by the source materials for biochar production. Similar results were reported in other previous research. The NH<sub>4</sub><sup>+</sup> sorption capacities for cacao shell and corn cob biochars were 0.24 mg/g and 0.56 mg/g, respectively (Hale et al., 2013). However, the NH<sub>4</sub><sup>+</sup> sorption capacities by hardwood shavings, rice husk and wood biochars were 5.3 mg/g, 39.8 mg/g, and 44.64 mg/g, respectively (Kizito et al., 2015). In this study, by comparison, the biochars presented a moderate sorption capacity. The  $q_{\max}$  of PCB300 (3.21 mg/g) was 2.7 times than that of PCB700 (1.78 mg/g), indicating a higher NH<sub>4</sub><sup>+</sup> sorption capacity for PCB biochar produced at 300 °C than at 700 °C. Therefore, the NH<sub>4</sub><sup>+</sup> sorption capacity of biochars can also be influenced by pyrolysis temperatures.

RSB300, SDB300 and ESB300 showed higher  $K_F$  compare to RSB700, SDB700 and ESB700, which indicated that the biochars produced at 300 °C presented higher NH<sub>4</sub><sup>+</sup> sorption capacity. In this study, the 1/n values were <1, suggesting there was a nonlinearity in the isotherms. Similar results were reported by Uchimiya et al. (2010).

The  $q_{\max}$  was positively correlated with Zeta potential with significance ( $p < 0.05$ ). A greater negative charge in the biochar produced at 300 °C than at 700 °C was found. The adsorptive capacity of NH<sub>4</sub><sup>+</sup> was hindered by the lower negative charges in ESB produced at the higher pyrolysis temperatures. Therefore, the higher NH<sub>4</sub><sup>+</sup> adsorption capacities were found in the biochars produced at lower pyrolysis temperatures, which was related to the greater negative charges. Our results agree with Takaya et al. (2016), who demonstrated that better NH<sub>4</sub><sup>+</sup> adsorption capacity was found for the biochars produced at lower pyrolysis temperatures due to increasing negatively-charged functional groups.

The  $q_{\max}$  was positively correlated with H/C content ( $p < 0.05$ ). Ahmad et al. (2014) found that the higher H/C ratio indicated the more sorption sites for inorganic contaminants. As presented in Table 2, the H/C ratio of biochar decreased under higher pyrolysis temperature, resulting in decreasing NH<sub>4</sub><sup>+</sup> adsorption. The  $q_{\max}$  of RSB, PCB and SDB was influenced by O content, O/C and (O + N)/C ratios of biochar (Fig. 4). Cui et al. (2016) showed that the highest O/C ratio and (O + N)/C ratio for *C. indica* biochar resulted in the largest sorption capacity for NH<sub>4</sub><sup>+</sup>. As shown in Table 2, the capacity adsorption NH<sub>4</sub><sup>+</sup> decreased with increasing pyrolysis temperatures for RSB, PCB and SDB, which was ascribed to the decrease in O/C and (O + N)/C ratios.

The capacity of NH<sub>4</sub><sup>+</sup> adsorption for ESB decreased with increasing pyrolysis temperatures, but its O/C and (O + N)/C ratios increased. This suggests that the mechanisms of NH<sub>4</sub><sup>+</sup> adsorption by ESB were different than those of RSB, PCB and SDB, and that this was related to their different functional groups. RSB, PCB and SDB presented the same band at 1616 cm<sup>-1</sup> (Mahtab et al., 2012),

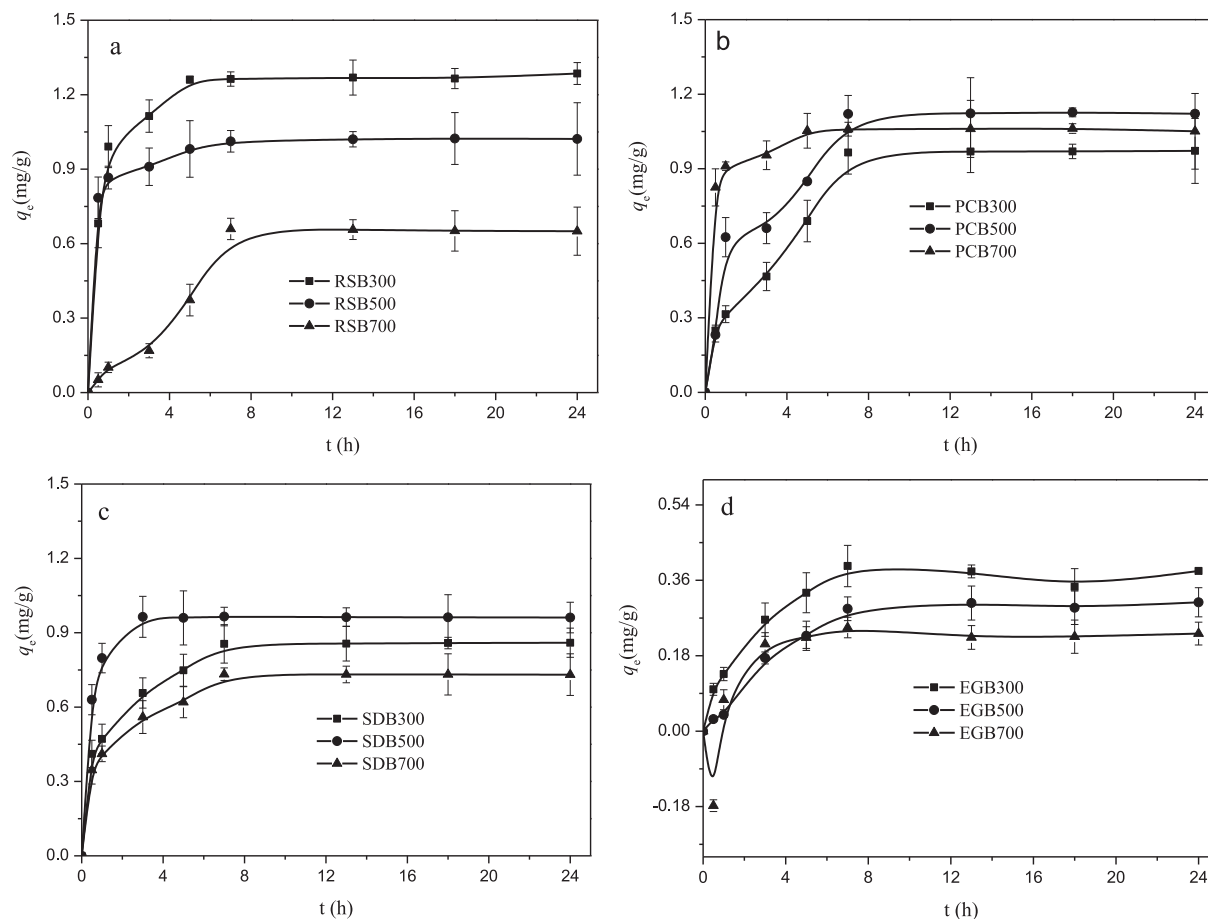


**Fig. 2.** Ammonia adsorption on the studied biochars over time. RSB300, RSB500 and RSB700 represent rice straw biochar produced at 300 °C, 500 °C and 700 °C, respectively. PCB300, PCB 500 and PCB700 represent *Phragmites communis* biochar produced at 300 °C, 500 °C and 700 °C, respectively. SDB300, SDB500 and SDB700 represent sawdust biochar produced at 300 °C, 500 °C and 700 °C, respectively; ESB300, ESB500 and ESB700 represent egg shell biochar produced at 300 °C, 500 °C and 700 °C, respectively. Data are means  $\pm$  SD (n = 3).

**Table 4**

Kinetic parameters of ammonium sorption on the biochars for different models.

Biochar	Pseudo-first-order			Pseudo-second-order			Intra-particle diffusion		
	$K_1$ (h <sup>-1</sup> )	$q_e$ (mg/g)	R <sup>2</sup>	$K_2$ (g/mg/h)	$q_e$ (mg/g)	R <sup>2</sup>	$K_3$ (mg/g/h <sup>0.5</sup> )	C (mg/g)	R <sup>2</sup>
RSB300	0.003	0.228	0.628	0.037	1.301	1.000	0.015	0.841	0.601
RSB500	0.004	0.177	0.898	0.063	1.040	1.000	0.007	0.814	0.781
RSB700	0.004	0.533	0.666	0.002	0.966	0.879	0.021	0.019	0.822
PCB300	0.006	0.797	0.837	0.016	1.025	0.998	0.024	0.202	0.822
PCB500	0.006	0.841	0.880	0.018	1.227	0.994	0.025	0.352	0.767
PCB700	0.003	0.130	0.699	0.076	1.078	1.000	0.007	0.864	0.711
SDB300	0.006	0.404	0.868	0.025	0.893	0.999	0.014	0.432	0.778
SDB500	0.005	0.123	0.746	0.134	0.970	1.000	0.007	0.751	0.483
SDB700	0.004	0.285	0.746	0.026	0.768	0.999	0.012	0.365	0.795
ESB300	0.003	0.193	0.471	0.033	0.397	0.991	0.008	0.126	0.687
ESB500	0.004	0.220	0.694	0.008	0.391	0.939	0.009	0.027	0.792
ESB700	0.003	0.109	0.592	0.230	0.234	0.988	0.009	0.016	0.469

RSB300, RSB500 and RSB700 represent rice straw biochar produced at 300 °C, 500 °C and 700 °C, respectively. PCB300, PCB500 and PCB700 represent *phragmites communis* biochar produced at 300 °C, 500 °C and 700 °C, respectively. SDB300, SDB500 and SDB700 represent sawdust biochar produced at 300 °C, 500 °C and 700 °C, respectively; ESB300, ESB500 and ESB700 represent egg shell biochar produced at 300 °C, 500 °C and 700 °C, respectively.

which represented the C=C and C=O stretching in the aromatic ring (Fig. 4a–c). In addition, the peak of 1077 cm<sup>-1</sup> was assigned to –OCH<sub>3</sub> (Wang et al., 2015). The peak of 1616 cm<sup>-1</sup> decreased after NH<sub>4</sub><sup>+</sup> adsorption indicating that these oxygen-containing functional groups were involved in NH<sub>4</sub><sup>+</sup> sorption. The peaks of 875 cm<sup>-1</sup> (Wang et al., 2018) and 1420 cm<sup>-1</sup> (Mahtab et al., 2012) of ESB were assigned to C–O groups and inorganic CO<sub>3</sub><sup>2-</sup>,

respectively. The 1420 cm<sup>-1</sup> peak decreased after NH<sub>4</sub><sup>+</sup> adsorption indicating NH<sub>4</sub><sup>+</sup> reaction with CO<sub>3</sub><sup>2-</sup> (Fig. 4d). Therefore, the NH<sub>4</sub><sup>+</sup> adsorption mechanisms in ESB were different than those in RSB, PCB and SDB.

Capacity of NH<sub>4</sub><sup>+</sup> adsorption can be influenced by pH. Decrease in NH<sub>4</sub><sup>+</sup> adsorption at pH > 8 might occur because it can be converted to NH<sub>3</sub> (Huang et al. 2010). In this study, the lowest capacity

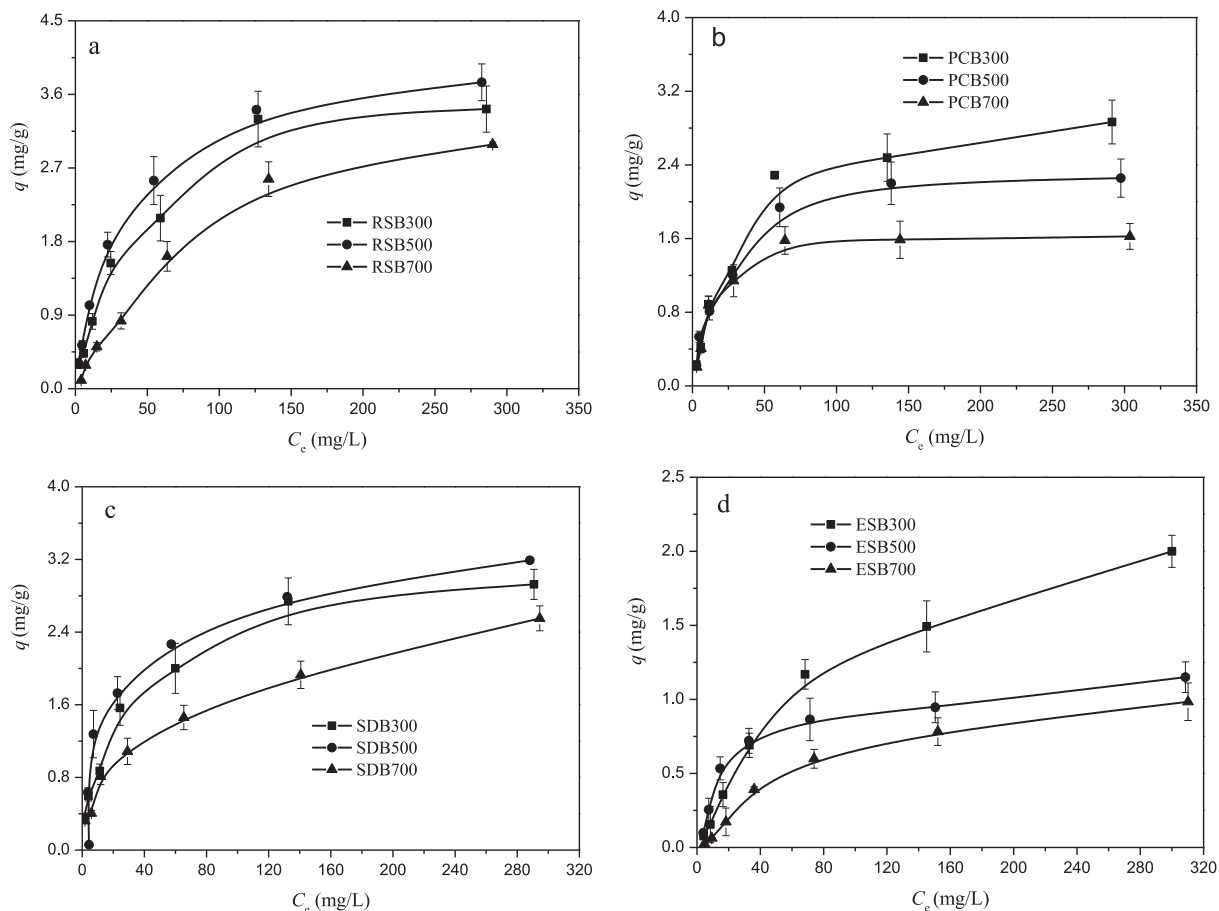


**Fig. 3.** Sorption isotherm of ammonium on the studied biochars. RSB300, RSB500 and RSB700 represent rice straw biochar produced at 300 °C, 500 °C and 700 °C, respectively. PCB300, PCB500 and PCB700 represent *Phragmites communis* biochar produced at 300 °C, 500 °C and 700 °C, respectively. SDB300, SDB500 and SDB700 represent sawdust biochar produced at 300 °C, 500 °C and 700 °C, respectively; ESB300, ESB500 and ESB700 represent egg shell biochar produced at 300 °C, 500 °C and 700 °C, respectively. Data are means  $\pm$  SD ( $n = 3$ ).

**Table 5**

Sorption parameters of ammonium on the biochars obtained from the Langmuir and Freundlich isotherm model.

Biochar	Langmuir			Freundlich		
	$q_{max}$ (mg/g)	$K_L$ (L/mg)	$R^2$	$K_F$ (mg/g)	$n$	$R^2$
RSB300	4.090	0.022	0.983	0.370	2.427	0.930
RSB500	4.175	0.032	0.998	0.496	2.670	0.942
RSB700	3.654	0.010	0.969	0.151	1.848	0.950
PCB300	3.206	0.025	0.982	0.374	2.668	0.906
PCB500	2.522	0.041	0.984	0.395	3.062	0.892
PCB700	1.776	0.068	0.972	0.396	3.692	0.811
SDB300	3.169	0.038	0.979	0.468	2.960	0.954
SDB500	3.300	0.048	0.934	0.507	2.958	0.878
SDB700	2.696	0.024	0.993	0.277	2.548	0.951
ESB300	2.201	0.010	0.994	0.101	1.882	0.964
ESB500	1.713	0.044	0.974	0.188	3.066	0.893
ESB700	1.288	0.011	0.990	0.038	1.721	0.882

RSB300, RSB500 and RSB700 represent rice straw biochar produced at 300 °C, 500 °C and 700 °C, respectively. PCB300, PCB500 and PCB700 represent *Phragmites communis* biochar produced at 300 °C, 500 °C and 700 °C, respectively. SDB300, SDB500 and SDB700 represent sawdust biochar produced at 300 °C, 500 °C and 700 °C, respectively; ESB300, ESB500 and ESB700 represent egg shell biochar produced at 300 °C, 500 °C and 700 °C, respectively.

of  $NH_4^+$  adsorption was found in the biochars produced at 700 °C with  $pH > 8$ .

As summarized in Tables 5 and 3, capacities of  $NH_4^+$  adsorption were higher for the biochars produced at 300 °C than those at 700 °C. However, surface area was lower for the biochars produced at 300 °C than those at 700 °C. The results indicate that surface area of the biochars did not obviously influence the  $NH_4^+$  adsorption

capacity. This agrees with Takaya et al. (2016), who demonstrated that biochars made from five feedstock (oak wood, commercial oak wood, greenhouse waste, municipal waste and presscake from AD) with high surface areas did not possess better ammonium adsorption capacities than low surface area chars; and suggests that surface area was not the most important factor influencing char ammonium adsorption capacity. Li et al. (2018) reported that max-

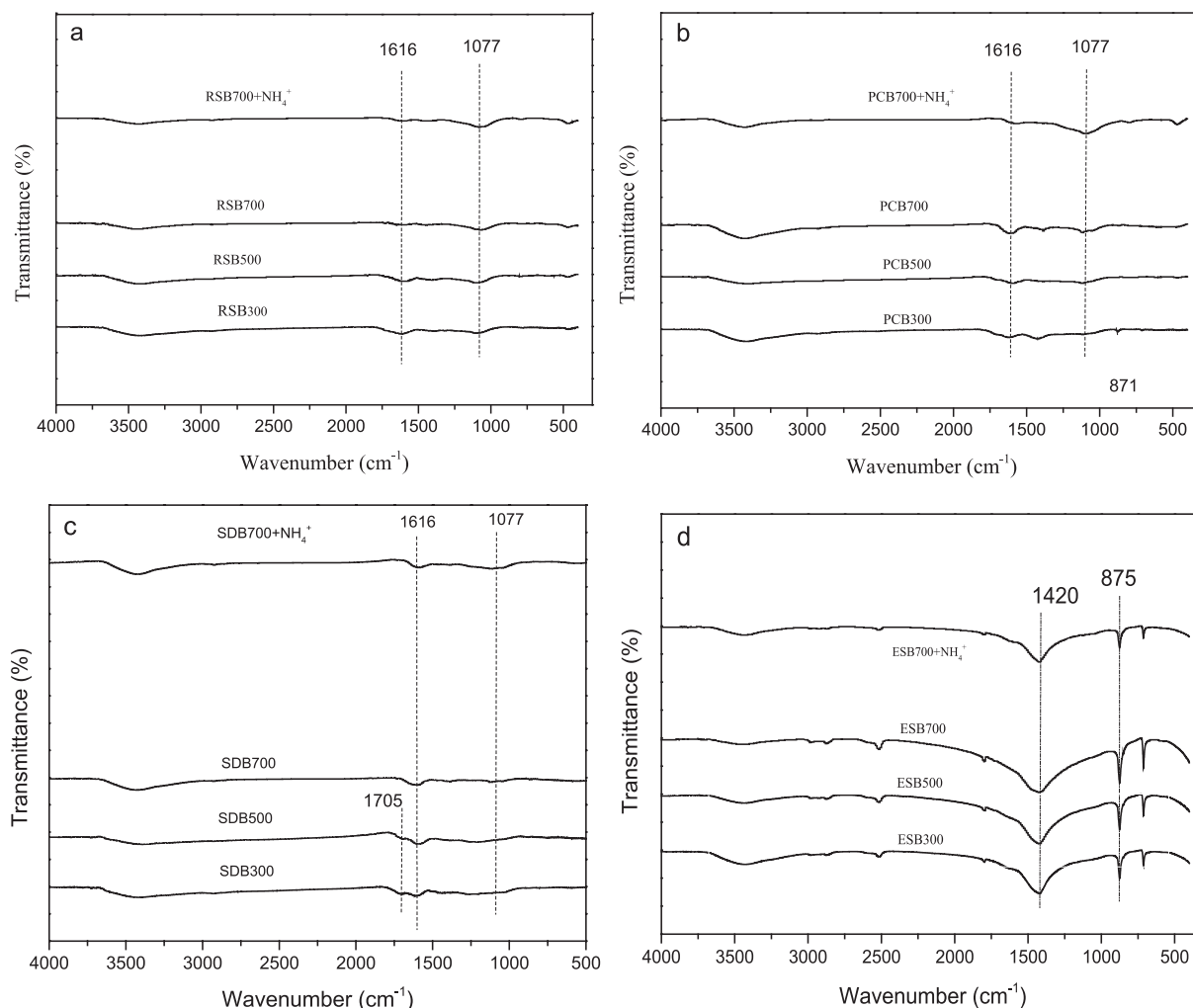


**Fig. 4.** FTIR spectra of the studied biochars. RSB300, RSB500 and RSB700 represent rice straw biochar produced at 300 °C, 500 °C and 700 °C, respectively. PCB300, PCB500 and PCB700 represent *Phragmites communis* biochar produced at 300 °C, 500 °C and 700 °C, respectively. SDB300, SDB500 and SDB700 represent sawdust biochar produced at 300 °C, 500 °C and 700 °C, respectively; ESB300, ESB500 and ESB700 represent egg shell biochar produced at 300 °C, 500 °C and 700 °C, respectively. RSB700 + NH<sub>4</sub><sup>+</sup>, PCB700 + NH<sub>4</sub><sup>+</sup>, SDB700 + NH<sub>4</sub><sup>+</sup>, and ESB700 + NH<sub>4</sub><sup>+</sup> represent loading NH<sub>4</sub><sup>+</sup> on RSB700, PCB700, SDB700 and ESB, respectively.

imum adsorption NH<sub>4</sub><sup>+</sup> was significantly correlated with cation exchange capacity (CEC) and micropore volume, but it was not significantly correlated with specific surface area, mesopore volume and pore size. Therefore, our result was also similar to those of Li et al. (2018), who found that surface area did not significantly influence biochar NH<sub>4</sub><sup>+</sup> adsorption.

### 3.6. Adsorption thermodynamics

As shown in Table 6, the values of  $\Delta S^\circ$  for RSB, PCB, SDB and ESB were 0.12, 0.20, 0.16 and 0.10, respectively, indicating increased disorder reaction. The results were similar to the studies of Hema and Arivoli (2007), who indicated that the disorder increased when  $\Delta S^\circ > 0$ . The values of  $\Delta G^\circ$  were in a range of  $-11.06$  to  $-16.12$  kJ/mol indicating a spontaneous process. The results were similar to other previous studies. The NH<sub>4</sub><sup>+</sup> adsorption on the biochars was a spontaneous process when  $\Delta G^\circ < 0$  (Qu et al., 2008; Simon et al., 2015). The values of  $\Delta H^\circ$  for RSB, PCB, SDB and ESB were 20.69, 46.27, 33.21 and 19.04, respectively, indicating that endothermic process occurred for NH<sub>4</sub><sup>+</sup> adsorption. The pseudo-second-order model has been used, implying a mechanism of chemical reactions (Wang et al., 2015). Therefore, the kinetic

**Table 6**  
Thermodynamic parameters for NH<sub>4</sub><sup>+</sup> adsorption on the biochars.

Biochar	T (K)	$\Delta H^\circ$ (kJ/mol)	$\Delta S^\circ$ (kJ/mol/K)	$\Delta G^\circ$ (kJ/mol)
RSB500	293	20.69	0.12	-13.78
	303			-15.37
	313			-16.12
PCB300	293	46.27	0.20	-11.90
	303			-14.76
	313			-15.85
SDB500	293	33.21	0.16	-12.90
	303			-14.45
	313			-16.05
ESB300	293	19.04	0.10	-11.06
	303			-11.91
	313 K			-13.12

RSB500 represent rice straw biochar produced at 500 °C. PCB300 represent *Phragmites communis* biochar produced at 300 °C. SDB500 represent sawdust biochar produced at 500 °C. ESB300 represent egg shell biochar produced at 300 °C.

data of this study indicate that NH<sub>4</sub><sup>+</sup> adsorption process was mainly through chemical reactions. In addition, the surface area of the biochar in this study was not the most important factor affecting NH<sub>4</sub><sup>+</sup> adsorption capacity.

#### 4. Conclusions

The characteristics of biochars were affected by feedstock types and pyrolysis temperatures, which consequently affected  $\text{NH}_4^+$  adsorption capacity. The maximum  $\text{NH}_4^+$  sorption was lower for the biochars produced in pyrolysis at 700 °C than at 300 °C or 500 °C. The capacities of  $\text{NH}_4^+$  sorption were higher for plant waste biochars (RSB, PCB and SDB) than those of ESB. Both the characteristics of biochars and the  $\text{NH}_4^+$  adsorption capacities were influenced by pyrolysis temperatures and feedstock materials. The  $\text{NH}_4^+$  sorption capacity was mainly influenced by zeta potential and C/H of the biochars.

#### Acknowledgements

This work was supported the Key Laboratory of Agro-Environment in downstream of Yangze Plain, Ministry of Agriculture, P. R. China (AE2018001), National Natural Science Foundation of China (Grant No. 40901257), Six talent peaks project in Jiangsu Province (JNHB-057), and Qing Lan Project (20161507).

#### References

- Ahmad, M., Lee, S.S., Dou, X., Mohan, D., Sung, J.K., Yang, J.E., Ok, Y.S., 2012. Effects of pyrolysis temperature on soybean stover and peanut shell-derived biochar properties and TCE adsorption in water. *Bioresour. Technol.* 118, 536–544.
- Ahmad, M., Rajapaksha, A.U., Lim, J.E., Zhang, M., Bolan, N., Mohan, D., Vithanage, M., Lee, S.S., Ok, Y.S., 2014. Biochar as a sorbent for contaminant management in soil and water: a review. *Chemosphere* 99, 19–33.
- Anastasakis, K., Ross, A.B., Jones, J.M., 2011. Pyrolysis behavior of the main carbohydrates of brown macro-algae. *Fuel* 90, 598–607.
- Bagreev, A., Bandosz, T., Locke, D., 2001. Pore structure and surface chemistry of adsorbents obtained by pyrolysis of sewage sludge-derived fertilizer. *Carbon* 39, 1971–1979.
- Chen, B., Zhou, D., Zhu, L., 2008. Transitional adsorption and partition of nonpolar and polar aromatic contaminants by biochars of pine needles with different pyrolytic temperatures. *Environ. Sci. Technol.* 42, 5137–5143.
- Chen, T., Zhang, Y., Wang, H., Lu, W., Zhou, Z., Zhang, Y., Ren, L., 2014. Influence of pyrolysis temperature on characteristics and heavy metal adsorptive performance of biochar derived from municipal sewage sludge. *Bioresour. Technol.* 164, 47–54.
- Chun, Y., Sheng, G., Chiou, C.T., Xing, B., 2004. Compositions and sorptive properties of crop residue-derived chars. *Environ. Sci. Technol.* 38, 4649–4655.
- Conley, D.J., Paerl, H.W., Howarth, R.W., Boesch, D.F., Seitzinger, S.P., Havens, K.E., Lancelot, C., Likens, G.E., 2009. Ecology controlling eutrophication: nitrogen and phosphorus. *Science* 323, 1014–1015.
- Cui, X.Q., Hao, H.L., Zhang, C.K., He, Z.L., Yang, X.E., 2016. Capacity and mechanisms of ammonium and cadmium sorption on different wetland-plant derived biochars. *Sci. Total Environ.* 539, 566–575.
- Fang, C., Zhang, T., Li, P., Jiang, R.F., Wang, Y.C., 2014. Application of magnesium modified crop biochar for phosphorus removal and recovery from swine wastewater. *Int. J. Environ. Res. Public Health* 11, 9217–9237.
- Hale, S.E., Alling, V., Martinsen, V., Mulder, J., Breedveld, G.D., Cornelissen, G., 2013. The sorption and desorption of phosphate-P, ammonium-N and nitrate-N in cacao shell and corn cob biochars. *Chemosphere* 91, 1612–1619.
- He, J.W., Yang, S.M., Zhang, G.Y., 2016. Recent studies on eggshell as adsorption material. *Trans. Chin. Soc. Agric. Eng.* 32, 297–303.
- Hema, M., Arivoli, S., 2007. Comparative study on the adsorption kinetics and thermodynamics of dyes onto acid activated low cost carbon. *Int. J. Phys. Sci.* 2, 10–17.
- Huang, H., Xiao, X., Yan, B., Yang, L., 2010. Ammonium removal from aqueous solutions by using natural Chinese (Chende) zeolite as adsorbent. *J. Hazard Mater.* 175, 247–252.
- Jin, J.W., Li, Y.A., Zhang, J.Y., Wu, S.C., Cao, Y.C., Liang, P., Zhang, J., Wong, M.H., Wang, M.Y., Shan, S.D., Christie, P., 2016. Influence of pyrolysis temperature on properties and environmental safety of heavy metals in biochars derived from municipal sewage sludge. *J. Hazard Mater.* 320, 417–426.
- Joseph, S.D., Downie, A., Crosby, A., Lehmann, J., Munroe, P., 2007. Biochar for carbon sequestration, reduction of greenhouse gas emissions and enhancement of soil fertility: a review of the materials science. *Rend. Circ. Mat. Palermo Suppl.* 48, 101–106.
- Jung, K.W., Kim, K., Jeong, T.U., Ahn, K.H., 2016. Influence of pyrolysis temperature on characteristics and phosphate adsorption capability of biochar derived from waste-marine macroalgae (*Undaria pinnatifida* roots). *Bioresour. Technol.* 200, 1024–1028.
- Kizito, S., Wu, S., Kirui, W.K., Lei, M., Lu, Q., Bah, H., Dong, R., 2015. Evaluation of slow pyrolyzed wood and rice husks biochar for adsorption of ammonium nitrogen from piggery manure anaerobic digestate slurry. *Sci. Total Environ.* 505, 102–112.
- Li, H.B., Dong, X.L., Evandro, B.S., Letuzia, M.O., Chen, Y.S., Lena, Q.M., 2017a. Mechanisms of metal sorption by biochars: biochar characteristics and modifications. *Chemosphere* 178, 466–478.
- Li, R., Wang, J.J., Zhou, B., Zhang, Z., Liu, S., Lei, S., Xiao, R., 2017b. Simultaneous capture removal of phosphate, ammonium and organic substances by MgO impregnated biochar and its potential use in swine wastewater treatment. *J. Clean Prod.* 147, 96–107.
- Li, S.M., Vanessa, B., Li, R.W., Chen, G., Yuch, P.H., 2018. Nitrogen retention of biochar derived from different feedstocks at variable pyrolysis temperatures. *J. Anal. Appl. Pyrol.* 133, 136–146.
- Loganathan, P., Vigneswaran, S., Kandasamy, J., Bolan, N.S., 2014. Removal and recovery of phosphate from water using sorption. *Crit. Rev. Env. Sci. Technol.* 44, 847–907.
- Mahtab, A., Lee, S.S., Dou, X.M., Dinesh, M., Sung, J.K., Jae, E.Y., Yong, S.O., 2012. Effects of pyrolysis temperature on soybean stover- and peanut shell-derived biochar properties and TCE adsorption in water. *Bioresour. Technol.* 118, 536–544.
- Ministry of Environmental Protection P.R.C., 2006. Monitoring and Analytical Methods of Water and Wastewater. China Environmental Science Press, Beijing, China.
- Qiu, X., Duan, L., Chai, F., Wang, S., Yu, Q., Wang, S., 2016. Deriving high-resolution emission inventory of open biomass burning in China based on satellite observations. *Environ. Sci. Technol.* 50, 11779–11786.
- Qu, B., Zhou, J., Xiang, X., Zheng, C., Zhao, H., Zhou, X., 2008. Adsorption behavior of Azo Dye C. I. Acid Red 14 in aqueous solution on surface soils. *J. Environ. Sci.* 20, 704–709.
- Simon, K., Wu, S.B., Kirui, W.K., Lei, M., Lu, Q.M., Bah, H.D., Dong, R.J., 2015. Evaluation of slow pyrolyzed wood and rice husks biochar for adsorption of ammonium nitrogen from piggery manure anaerobic digestate slurry. *Sci. Total Environ.* 505, 102–112.
- Smith, V.H., 2003. Eutrophication of freshwater and coastal marine ecosystems a global problem. *Environ. Sci. Pollut. R.* 10, 126–139.
- Sun, K., Ro, K., Guo, M., Novak, J., Mashayekhi, H., Xing, B., 2011. Sorption of bisphenol A, 17alpha-ethinyl estradiol and phenanthrene on thermally and hydrothermally produced biochars. *Bioresour. Technol.* 102, 5757–5763.
- Takaya, C.A., Fletcher, L.A., Singh, S., Anyikude, K.U., Ross, A.B., 2016. Phosphate and ammonium sorption capacity of biochar and hydrochar from different wastes. *Chemosphere* 145, 518–527.
- Tan, I.A., Ahmad, A., Hameed, B.H., 2008. Adsorption of basic dye on high-surface-area activated carbon prepared from coconut husk: equilibrium, kinetic and thermodynamic studies. *J. Hazard Mater.* 154, 337–346.
- Tarpeh, W.A., Udert, K.M., Nelson, K.L., 2017. Comparing ion exchange adsorbents for nitrogen recovery from Source-Separated urine. *Environ. Sci. Technol.* 51, 2373–2381.
- Uchimiya, M., Wartelle, L.H., Lima, I.M., Klasson, K.T., 2010. Sorption of deisopropylatrazine on broiler litter biochars. *J. Agric. Food Chem.* 58, 12350–12356.
- Wang, S.D., Kong, L.J., Long, J.Y., Su, M.H., Diao, Z.H., Chang, X.Y., Chen, D.Y., Song, G., Kaimin, S., 2018. Adsorption of phosphorus by calcium-flour biochar: isotherm, kinetic and transformation studies. *Chemosphere* 195, 666–672.
- Wang, Z., Liu, G., Zheng, H., Li, F., Ngo, H.H., Guo, W., Liu, C., Chen, L., Xing, B., 2015. Investigating the mechanisms of biochar's removal of lead from solution. *Bioresour. Technol.* 177, 308–317.
- Wang, Z., Nie, E., Li, J., Yang, M., Zhao, Y., Luo, X., Zheng, Z., 2011. Equilibrium and kinetics of adsorption of phosphate onto iron-doped activated carbon. *Environ. Sci. Pollut. Res. Int.* 19, 2908–2917.
- Yao, Y., Gao, B., Zhang, M., Inyang, M., Zimmerman, A.R., 2012. Effect of biochar amendment on sorption and leaching of nitrate, ammonium, and phosphate in a sandy soil. *Chemosphere* 89, 1467–1471.
- Yin, Q.Q., Wang, R.K., Zhao, Z.H., 2018. Application of Mg-Al-modified biochar for simultaneous removal of ammonium, nitrate, and phosphate from eutrophic water. *J. Clean Prod.* 176, 230–240.
- Yuan, J.H., Xu, R.K., Zhang, H., 2011. The forms of alkalis in the biochar produced from crop residues at different temperatures. *Bioresour. Technol.* 102, 3488–3497.
- Zhang, H., Voroney, R.P., Price, G.W., 2015a. Effects of temperature and processing conditions on biochar chemical properties and their influence on soil C and N transformations. *Soil Biol. Biochem.* 83, 19–28.
- Zhang, J., Liu, J., Liu, R., 2015b. Effects of pyrolysis temperature and heating time on biochar obtained from the pyrolysis of straw and lignosulfonate. *Bioresour. Technol.* 176, 288–291.
- Zhang, J.S., Wang, Q.Q., 2016. Sustainable mechanisms of biochar derived from brewers' spent grain and sewage sludge for ammonia-nitrogen capture. *J. Clean Prod.* 112, 3927–3934.